PHANTOM DOSIMETRY AND IMAGE QUALITY OF GALILEOS COMFORT PLUS CONE BEAM COMPUTED TOMOGRAPHY

Ross D. Hunter

A thesis submitted to the faculty at the University of North Carolina at Chapel Hill in partial fulfillment of the requirements for the degree of Master of Science in the School of Dentistry (Orthodontics).

Chapel Hill
2014

Approved by:

John B. Ludlow

Tung T. Nguyen

Lorne D. Koroluk

ABSTRACT

Ross D. Hunter: Phantom Dosimetry and Image Quality of Galileos Comfort PLUS Cone Beam Computed Tomography
(Under the direction of John B. Ludlow)

Introduction: Increasing use of CBCT in many aspects of dental treatment has been associated with an elevated concern for the long-term risks of x-ray exposure, especially in adolescent patients. An industry response to this has been to offer lower-exposure and collimated field scanning options. **Methods:** Effective doses resulting from various combinations of field size/location (FOV), number of image frames, and mAs settings were calculated for ATOM child and adult anthropomorphic phantom exposures using the Galileos Comfort Plus CBCT unit. Optical Stimulated Dosimetry was used with a previously validated protocol. Image quality data was acquired with the Quart DVT CBCT phantom. **Results:** For the same exposures, child doses averaged 32% greater than adult ($p=0.0004$). Full field doses were greater than mandibular followed by maxillary ($p=0.0002$). Dose increased with increasing mAs ($p>0.0001$). Increasing Contrast Noise Ratio (CNR) was associated with increasing mAs ($p=0.0106$) and frames ($p=0.0423$), while Modulation Transfer Function (MTF) was not ($p>0.05$). **Conclusions:** An average of 66% reduction in dose can be achieved when using standard exposure parameters in comparison with high-definition exposures. CNR was correlated with increasing dose; however, the clinical implication of this requires further study.

ACKNOWLEDGEMENTS

Thank you to my committee members, Dr. John Ludlow, Dr. Tung Nguyen, and Dr. Lorne Koroluk, for their expertise, guidance, and advice throughout my project. Thank you to Dr. Jacob Dunn for his assistance with data collection. Thank you to the NIDCR for their research grant. Most importantly, thank you to my wife, Jennifer, and children, Julia, Natalie, and Dean, for their unending love and support.

TABLE OF CONTENTS

LIST OF TABLES

LIST OF FIGURES

LITERATURE REVIEW

The use of ionizing radiation in diagnostic medical examinations has increased over the last 20 years to the point where the annual per capita dose to the US population from all sources has doubled.[1] The risk of this exposure is notable, and it has been estimated that from 1.5% to 2% of all US cancers may be attributed to computed tomography (CT) studies alone.[2] Cancer, being the principal long-term effect of exposure to x-rays, makes this issue an important one. Evidence indicates that an adult exposure to x-rays as low as 90 millisieverts (mSv) or a fetal exposure of 9-20 mSv is a cancer risk. A linear-no-threshold hypothesis of x-ray risk fits most data for cancer development, but extrapolation of this data must be used to estimate risks from the lower doses that are utilized for diagnostic imaging. The majority of scientists working in this area accept this extrapolation as reasonable and prudent.[3] Although the risk to an individual from a single exam may not itself be large, millions of exams are performed each year, making radiation exposure from medical imaging an important public health issue.

A routine CT head scan may have an effective dose of approximately 2 mSv.[4] Cone beam computed tomography (CBCT) examinations have been reported to impart a fraction of this dose; however, scans from some units approach 1 mSv, and scans from other units have been shown to be equivalent in dose to optimized CT scans.[5] This range of differences is especially important when considering the pediatric and adolescent populations, because cellular growth and organ development is associated with increased radiosensitivity of tissues. In conjunction

with a longer life expectancy in which cancer can develop, children are two to five times more sensitive to radiation carcinogenesis than mature adults.[4, 6]

The biological effect of exposure to ionizing radiation, expressed as the risk of cancer development over a lifetime, is determined from absorbed radiation dose in combination with other factors that account for differences in exposed tissue sensitivity and other patient susceptibility factors such as gender and age. Simple measurement of absorbed ionizing radiation does not account for sensitivity of tissues or other factors important for determining risk. To address this issue, the International Commission on Radiological Protection (ICRP) suggested in 1990 that effective dose (*E*) be adopted as the best means of comparing dose and risk from any exposure to ionizing radiation.[7] Effective dose was created to provide a dose quantity related to the probability of health detriment due to stochastic effects of exposure to low doses of ionizing radiation. Organs and tissues known to be most susceptible to radiation damage were assigned weights that represent the relative contribution of each tissue to overall risk. Effective dose, reported in sieverts, was defined as the sum of the products of each tissue-weighting factor (w_T) and the equivalent dose to that tissue (H_T), $E = \Sigma\, w_T \times H_T$.

In 2007, the ICRP published a revision of the tissue-weighting factors used in the calculation of effective dose.[8] This was made possible by the availability of cancer incidence data that was not available when the 1990 guidelines were published. The 1990 ICRP cancer risks were computed based on mortality data. Incidence data provided a more complete description of cancer burden than mortality data alone, particularly for cancers that have a high survival rate. Much of the cancer incidence data came from the Life Span Study of Japanese atomic bomb survivors, which had been updated with follow-up through 1998 and corrected using DS86 bomb dosimetry. Weighted tissues and organs and revised weights in the 2007

recommendations were justified because of accumulated epidemiologic information on the tumorigenic effects of radiation that was sufficient to make judgments necessary for estimating cancer risks. Cancer risk in salivary glands and brain were judged to be greater than that of other tissues in the remainder fraction, and each was ascribed a w_T of 0.01. A w_T value for the remainder tissues of 0.12, distributed equally among 13 of 14 named tissues, provided a weight of approximately 0.009 each, which was just marginally lower than the w_T for the lowest of the named tissues. Of significance for maxillofacial imaging, there was an increase in the risk estimation for brain tissues and the addition of salivary glands, oral mucosa, and lymph nodes, which may be partially or fully irradiated during maxillofacial examinations. These changes in the calculation of risk from x-ray exposures to the head and neck area prescribed by ICRP have resulted in increases in estimated risk to adult patients by as much as 422% from previously used 1990 calculations.[9]

A dramatic increase in the use of CBCT has occurred in dentistry during the last decade. CBCT allows the acquisition of three-dimensional volumes of the dental arches and surrounding tissues at a high spatial resolution and a low radiation dose. There are a number of different dental applications that benefit from the use of CBCT, each with specific requirements regarding the size of the acquired volume and the image quality in terms of spatial and contrast resolution.[10] Some have already declared it the new "gold standard" of maxillofacial imaging and predict that it will be used by most dental practices within the next decade.[11]

Along with many other areas of dental practice, CBCT technology has found application in orthodontic diagnosis and treatment planning.[12-18] However, one of the greatest issues facing the use of CBCT in orthodontics is justification of the increased doses of ionizing radiation administered to patients compared with standard two-dimensional imaging techniques. Modern

digital panoramic and cephalometric radiographs have been reported to administer effective doses of 14-24 μSv and 4-5 μSv, respectively.[9, 19] As stated earlier, a routine medical CT head scan can have an effective dose of approximately 2 mSv, whereas most CBCT units have been reported to impart a much lower dose.[2] Available CBCT units from different manufacturers have been shown to vary in dose by as much as 10-fold for an equivalent field of view (FOV) examination.[5] In fact, for a large FOV scan, effective dose can range from 68 to 1073 μSv. In addition, adjustments of exposure factors to improve image quality are available in many CBCT units and can cause as much as a 7-fold increase in patient dose.[5]

Recently, Pauwels and his colleagues examined the effective dose range on 14 CBCT scanners, using different exposure protocols and geometries.[20] Their results displayed a range from 19 to 368 μSv, illustrating a 20-fold range. The effective doses for the large FOV scans ranged between 68 and 368 μSv. The effective doses for the medium FOV scans were from 28 to 265 μSv. Lastly for the small FOV scans, the effective doses ranged between 19 and 44 μSv. The largest contributors to the effective dose were from the remainder tissues (adipose tissue, extrathoracic region, lymphatic nodes, muscle, and oral mucosa), followed by the salivary glands and thyroid gland. Contributions of the brain, bone surface, and skin were almost negligible. Interestingly, Pauwels et al. used a large amount of dosimeters to collect the absorbed radiation data (147 for one phantom, 152 for another phantom), trying to get an even spread over each of the radiosensitive organs in the head and neck regions and produce dose estimates that were as accurate as possible. Ludlow responded that while this was a laudable goal, sampling strategy is just one of a number of factors that are important in measuring dose.[21] Just as important are the actual location and extent of the radiosensitive organs that are being measured and the location of the field of view when exposing the phantom. He pointed out that results for the NewTom

VGi were almost double that of his findings, which were probably due to poor positioning of the phantom, causing the thyroid gland to be directly exposed. Ludlow also stated that while the use of additional dosimeters may increase the precision of calculation of organ dose, it does not guarantee an increase in the accuracy of the calculation of effective dose. He recommended the development of phantoms that can provide reasonable indicators of effective dose with fewer, rather than more dosimeters.

In their conclusions, Pauwels et al. stated that further study is required to bring image quality into play, on a technical and diagnostic level.[20] By investigating technical image quality, the relation between the exposure from CBCT units and the image quality performance in terms of noise, sharpness, contrast and artifacts, diagnostic quality studies could link all quantifications of dose and image quality to performance evaluation on a clinical level. Ludlow and Walker explained that because image quality is subjective, the measurement and comparison of image quality across CBCT units in diagnostic situations pose complex problems.[22] Two elements of subjective image quality that correlate with objective quality measures include contrast and spatial resolution.[23] Image contrast can be objectively measured with the contrast-to-noise ratio, and spatial resolution can be measured by computing a modulation transfer function.

As Ludlow and Walker pointed out, the ongoing challenge in the optimization of CBCT is to reduce the dose without drastically decreasing image quality and diagnostic information.[22] Image quality technical-factor adjustments that select between "high" and "low" image quality in many CBCT scanners can cause as much as a 7-fold difference in doses.[5] One possible way of reducing patient risk from CBCT examinations is to limit the area of exposure using variable FOVs that are sized for the location of the anatomy of interest. However, voxel size is linked to FOV in many CBCT units, and smaller voxel sizes associated with smaller FOVs can actually

increase the dose because of increases in exposure that are needed to maintain an adequate contrast-to-noise ratio.[22] Another potential means of reducing patient risk is to reduce exposure for diagnostic tasks that theoretically require lower contrast-to-noise ratios or lower signal modulation transfer functions. For example, checking the root angulation during mid-orthodontic treatment could apply. The combination of careful selection of exposure parameters and FOV can result in an optimal dose for specific diagnostic tasks in orthodontic practice. Contrast-to-noise ratio data in conjunction with modulation transfer function indications of resolution limits might be helpful guides in indicating the usefulness of different CBCT scanning parameters for specific diagnostic tasks. Determination of which exposure protocol is appropriate for a specific diagnostic task awaits further research.

In August of 2013, the American Academy of Oral and Maxillofacial Radiology (AAOMR) released a position statement on their clinical recommendations regarding the use of CBCT in orthodontic treatment.[24] At the beginning of the statement, they listed diagnostic uses of CBCT in orthodontics, which include dental structural anomalies[25-30], anomalies in dental position[31-34], compromised dento-alveolar boundaries[35-37], asymmetry[38-40], anteroposterior discrepancies[41-43], vertical discrepancies[44, 45], transverse discrepancies[44, 46], TMJ signs and/or symptoms[47-49], dentofacial deformities and craniofacial anomalies[50-52], conditions that affect airway morphology[53-55], specific surgical procedures, orthodontic mini-implants used as temporary anchorage devices[56-58], and maxillary expanders.[59, 60] Then, they suggested four guidelines regarding the use of CBCT in orthodontic treatment. First, image appropriately according to the clinical situation. In other words, the decision to perform a CBCT examination should be based on the patient's history, clinical examination, available radiographic imaging, and the presence of a clinical condition for which the benefits to the diagnosis and treatment plan

outweigh the risks of exposure to radiation, especially in the case of a child or young adult. They recommend avoiding the use of CBCT to obtain data that can be provided by alternative non-ionizing modalities, e.g., to produce virtual orthodontic study models. They also point out that few authors have presented higher levels of evidence and measured the impact of CBCT on orthodontic diagnosis and treatment planning decisions. One recent article looked at this topic and found that treatment plans were only affected in cases of unerupted teeth, severe root resorption, and severe skeletal discrepancies. No benefit was found in cases where CBCT scans were used to examine abnormalities of the temporomandibular joint, airway space, or dental crowding.[61] Another study conducted dosimetry of the SureSmile (OraMetrix, Richardson, TX) scan protocol using an i-CAT Next Generation CBCT unit.[19] They found that a SureSmile scan of both arches in an adult imparts an effective dose of 148 μSv. This would correspond to an effective dose of between 148 and 198 μSv for the average pediatric orthodontic patient, according to Ludlow and Walker.[22] No research has been conducted to validate enhanced treatment outcomes associated with the SureSmile protocol, in defense of its increased radiation exposure. This leads to the second guideline from the AAOMR.

The second guideline is to assess the radiation dose risk. Orthodontists must be knowledgeable of the radiation risk of performing CBCT scans and be able to communicate this risk to their patients. Because CBCT exposes patients to ionizing radiation that may pose elevated risks to some patients (pregnant or younger patients), orthodontists must explain and disclose to patients the radiation exposure risks, benefits, and alternatives. Third, they recommend minimizing the patient radiation exposure. Specifically, one should perform CBCT imaging with acquisition parameters adjusted to the nominal settings consistent with providing appropriate images of task-specific diagnostic quality for the desired diagnostic information.

Suggestions include using a pulsed exposure mode, optimizing exposure settings (mA, kVp), reducing the number of basis projection images, and employing dose reduction protocols (e.g., reduced resolution) when possible. Lastly, the AAOMR recommends maintaining professional competency in performing and interpreting CBCT studies. Orthodontists must be able to exercise judgment by applying professional standards to all aspects of CBCT, while improving their skills through lifelong learning in regards to the performance and interpretation of CBCT examinations.

INTRODUCTION

Since its introduction into dentistry in 1998, the use of cone beam computed tomography (CBCT) in orthodontics has increased tremendously.[17] Coupled with the increased use of CBCT has been the heightened concern regarding the long-term risks of ionizing radiation. Cancer is the principal long-term biologic effect of exposure to radiation. Thus, one of the major issues facing orthodontists today is the justification of the increased doses of ionizing radiation administered to patients via CBCT versus the traditional two-dimensional imaging techniques.

According to a 2007 review paper from the New England Journal of Medicine, an estimated 1.5% to 2% of all cancers in the United States may be attributable to the radiation from computed tomography (CT).[2] A routine medical CT examination of the head can have an effective dose of approximately 2 mSv.[4] Most CBCT examinations have been reported to produce a much lower dose; however, some CBCT units from various manufacturers differ in their doses by a factor of 10 for an equivalent field of view (FOV), with the higher doses being comparable to optimized CT scans.[5] Even though the risk to a patient from a single CT or CBCT examination may be low, millions of exams are performed each year, making radiation exposure from medical and dental imaging an important public health issue.

Radiation exposure is especially important for the pediatric and adolescent populations that are most often treated by orthodontists. The cellular growth and organ development seen in these populations are associated with increased radiosensitivity of tissues. In addition, these

patients have a longer life expectancy in which cancer can develop. Overall, children are two to five times more susceptible to radiation carcinogenesis than mature adults.[4, 6]

The quality of CBCT images is also an important factor for orthodontists to consider. CBCT image quality is observer dependent and subjective. Being subjective, the measurement and comparison of image quality across CBCT units are difficult to address. Two areas of subjective image quality that correlate with objective quality measures are contrast and spatial resolution. Image contrast has been objectively measured using the contrast-to-noise ratio, and spatial resolution has been measured by computing a modulation transfer function.[22] The quality of the CBCT scan is an important consideration for the orthodontist because of how it affects patient dose. It has been reported that making selections between "low" and "high" image quality in some CBCT units can cause a 7-fold increase in effective dose.[5] The challenge in the optimization of CBCT is to reduce the dose without drastically affecting image quality and diagnostic information. One potential way to reduce patient risk of ionizing radiation is to limit the area of exposure using variable FOVs that are appropriately sized for the anatomy of interest. However, as Ludlow and Walker pointed out, voxel size is linked to FOV in many CBCT units, and smaller voxel sizes associated with smaller FOVs can actually increase the dose because of increases in exposure that are necessary to maintain an adequate contrast-to-noise ratio.[22] Another potential way to decrease the risk is to reduce exposure for diagnostic tasks that do not require high contrast-to-noise ratios or signal modulation transfer functions. The combination of careful selection of FOV and exposure parameters can result in an optimal dose for the orthodontist's specific diagnostic task.

The purpose of this study was to evaluate doses resulting from various combinations of FOV size, location, and exposure parameters using child and adult phantoms with the Galileos

Comfort Plus CBCT unit (Sirona USA, Charlotte, NC). A second aim was to measure contrast-to-noise ratio and modulation transfer function as quantitative measurements of image quality for the various exposure options offered by the Galileos unit.

MATERIALS AND METHODS

The Galileos Comfort Plus CBCT unit (Sirona USA) was investigated in this study. Volume scans for this unit range from a 15 cm sphere for the full FOV, to a truncated sphere with a height of 8.5 cm for the maxillary and mandibular collimated FOVs. The unit operates at 98 kVp with a pulsed exposure. The unit rotates through a complete rotation angle of 180º over a scan time of 14 seconds. The voxel size for the unit is 0.25 cm^3. The transition from full FOV to collimated FOVs is accomplished using a simple mechanical switch on the unit. The unit also provides standard scans (HD off) with 200 basis images or high-definition scans (HD on) with 500 basis images.

Two head and neck phantoms were used in the study. Adult dosimetry was acquired using a tissue equivalent phantom simulating the anatomy of an average adult male (Atom Max Model 711 HN, CIRS Inc., Norfolk, VA). The phantom includes detailed 3D anthropomorphic anatomy including bone, brain, sinuses, nasal cavities, teeth, larynx, and a trachea. The bones contain both cortical and trabecular separation. The phantom was modified by making slots to accept Nanodot dosimeters at sites corresponding to internal tissues of interest. A skin surface dosimeter in the back of the neck was positioned at the vertical center of the designated slice level and taped in position. Lens of the eye dosimeters were centered over an inset in the anatomic location for the lens and taped in position. Internal dosimeters were positioned vertically with the upper edge of the dosimeter holder flush with the surface of the selected slice level and held in position by friction of the dosimeter case and the phantom material at the

sampled anatomic location. Adult phantom dosimeter anatomic locations and phantom levels are seen in Figure 1. During scanning, the phantom was oriented with the phantom section planes approximately parallel to the scan rotation plane, parallel to Frankfort horizontal. A phantom position simulating positioning of a patient on the chin rest was used.

Child dosimetry was acquired using a tissue equivalent phantom simulating the anatomy of a ten-year old child (Atom Model 706 HN, CIRS Inc., Norfolk, VA). Tissues simulated in this ATOM phantom include average bone tissue, average soft tissue, brain, sinuses, spinal cord, and spinal disks. Simulated bone tissue matches age-related density. Dosimeter anatomic locations and child phantom levels are seen in Figure 2. In addition, the scan parameters used for CBCT scans of the child and adult phantoms are given in Table 1.

Optically stimulated luminescent (OSL) dosimeters (Nanodot, Landauer, Inc., Glenwood, IL) were used to record the radiation doses. Each dosimeter was encased in a light-tight plastic holder measuring approximately 1 mm x 10 mm x 10 mm. This case prevented loss of energy through stimulation by ambient light. The OSL dosimeters were cleared and prepared for data collection by exposing them to a low UV emitting light source for 24 hours, in accordance with the manufacturer's instructions. The dosimeters were read using the portable MicroStar reader (Landauer, Inc., Glenwood, IL). The reader was calibrated before use. Following calibration, photon counts from dosimeters were recorded with an accuracy of about +/- 2%. Photon counts were converted to dose using an energy specific conversion factor. Doses reported by the reader were adjusted for energy response using a third-order polynomial calibration curve derived from side-by-side comparisons of recorded doses from an ion chamber and OSL dosimeters over a range of 80 – 120 kVp using an adjustable kVp source. For this study, the OSL sensitivity at 98

kVp was estimated at 0.91 (mean kV estimated as 66). Dividing recorded dosimeter value by energy sensitivity was used to calculate actual dose.

Two to ten exposures were utilized for each dosimeter run to provide a more reliable measure of radiation in the dosimeters. Collimated FOVs require more exposure repetition because more dosimeters are outside of the field of direct exposure and absorb only small quantities of scatter radiation. Doses recorded by the MicroStar reader were subsequently divided by the number of scans to determine the exposure per examination for each dosimeter.

Doses from the OSL dosimeters at different positions within a tissue or organ were averaged to express the average tissue-absorbed dose in micrograys (μGy). The products of these values and the percentage of a tissue or organ irradiated in a radiographic examination (Table 2) were used to calculate the equivalent dose (H_T) in microsieverts (μSv).[8]

For bone, the equivalent dose to the whole-body bone surface was calculated using the summation of the individual equivalent doses to the calvarium, the mandible, and the cervical spine. The determination of these equivalent doses is based on the distribution of bone throughout the body: the calvarium contains 11.8%, the mandible, 1.3%, and the cervical spine, 3.4%.[62] Distribution of adult bone marrow was calculated using an average of data from Christy for 25 and 40 year olds.[63] The calvarium contains 7.7%, the mandible, 0.8%, and the cervical spine, 3.8% of the adult marrow distribution. The 10 year-old child marrow distribution was calculated as 11.6% for the calvarium, 1.1% for the mandible, and 2.7% for the cervical spine, for a total of 15.4% of the total body marrow. Following the technique of Underhill et al,[62] three locations within the calvarium were averaged to determine calvarial dose. For bone, a correction factor based on experimentally determined mass energy attenuation coefficients for bone and

muscle irradiated with mono-energetic photons was applied. An effective beam energy estimated to be two-thirds of the peak beam energy of the x-ray unit was used to determine the bone-to-muscle attenuation ratios. A linear fit (R^2=0.996) of ratios from 40 to 80 kV from published data produced the following equation: bone-to-muscle attenuation ratio = -0.0618 x kV peak x 2/3 + 6.9406.[64] Values calculated from this equation provided a bone-to-muscle attenuation ratio of 2.88 at 66 kV (98 kV peak).

The proportion of skin surface area in the head and neck region directly exposed during maxillofacial CBCT imaging was estimated as 5% of the total body to calculate the radiation-weighted dose to the skin following the procedure from Ludlow et al.[65] Similarly, muscle and lymphatic nodes exposures were estimated to represent 5% of the total body complement for these tissues. The proportion of the esophageal tract that is exposed was set at 10%. Other tissues of interest were calculated at 100%.

The effective dose (E) is a calculation that permits comparison of the detriment of different exposures to ionizing radiation to an equivalent detriment produced by a full body dose of radiation. Effective dose, expressed in microsieverts, is calculated using the equation: $E = \sum w_T \times H_T$, where E is the summation of the products of the tissue weighting factor (w_T), which represents the relative contribution of that organ or tissue to the overall risk, and the radiation-weighted dose, H_T.[8] The whole-body risk is found by the summation of the radiation-weighted doses to all tissues or organs exposed. The International Commission on Radiological Protection (ICRP) weighting factors in Table 2 were used to calculate effective doses.[8] These factors included 14 independently weighted tissues and a group of 14 remainder tissues.[62] Since the uterus and cervix are present only in females, and the prostate only in males, the number used in the weighted averaging of the remainder tissues was 13.

Analysis of variance (ANOVA) of effective dose results was used to assess the data for significant differences due to phantom type (adult, child), collimation (maxillary, mandibular, full field), and scan protocol (HD on, HD off). Tukey's HSD test was used to determine which factors were significantly different from the others. An alpha value of 0.05 was chosen for all tests.

Image quality indicators associated with FOV, scanning angle, kilovolt peak, and voxel size were acquired using a QUART DVT_AP phantom and QUART DVT_TEC software (QUART, Zorneding, Germany) (Figure 3). The phantom consisted of 16-cm-diameter cylindrical slabs of acrylic plastic with polyvinyl chloride and air elements configured to permit measurements of polymethyl methacrylate (PMMA) voxel, PMMA noise, homogeneity, contrast, contrast-to-noise ratio, modulation transfer function 10%, modulation transfer function 50%, and Nyquist frequency. The measurements were calculated in a user-guided, semiautomatic manner from two DICOM slices selected from the volume. Each volume was measured three times, from which averages and standard deviations for each parameter were calculated.

RESULTS

The effective doses for the various combinations of parameters for the Galileos Comfort Plus CBCT unit are reported in Table 3. ANOVA of the combined child and adult phantom effective dose data demonstrated that for the same exposures, the child doses averaged 32% greater than the adult doses ($p = 0.0004$). These results are illustrated in Figures 4 and 5, with the high-definition setting turned on and off, respectively.

The Tukey's HSD test demonstrated that the effective doses from the full field of view scans were significantly greater than the mandibular field of view scans, followed by the maxillary field of view scans ($p = 0.0002$). These differences can be detected in Figures 6 through 9, corresponding to the phantom type and high-definition settings. The coefficient of determination values (R^2) in the figures range from 0.944 to 0.999, demonstrating a very high reproducibility of the experimental data.

Figures 4 through 9 also illustrate that as the mAs increased, so did the effective dose ($p < 0.0001$). This is why the effective doses continued to increase from the child setting up to the large adult setting. It also explains why the high-definition scans, with greater mAs values, corresponded to higher effective doses.

Figures 10 and 11 provide equivalent doses to tissues and organs used in the calculation of effective dose. Absorbed dose in the thyroid was significantly greater in the child phantom

than in the adult phantom ($p < 0.0001$) and comprised a greater percentage of the overall absorbed dose.

Table 4 contains average parameter values and standard deviations from the analysis of the QUART phantom images. As expected, increasing contrast-to-noise ratios were associated with increasing mAs ($p = 0.0106$) and basis images ($p = 0.0423$), while modulation transfer function was not ($p>0.05$).

DISCUSSION

In this study, we placed OSL dosimeters inside an adult ATOM phantom and a 10-year-old pediatric ATOM phantom to collect dosimetry data from the Galileos Comfort Plus CBCT unit. Ludlow and Walker validated the use of these dosimeters and phantoms, thus allowing these materials to provide data that are applicable to the majority of orthodontic patients.[22] What we found was that for the same exposure settings, effective doses were an average of 32% higher in the child phantom than in the adult phantom. Taking a closer look at the data, specifically the equivalent doses, reveals that the increase in effective dose in the child was mostly due to the simulated anatomic position of the thyroid (Figure 12). The values calculated for thyroid dose in the adult ATOM phantom were based on readings from two dosimeters positioned at level 10, where the bulk of the lobes and the isthmus of the thyroid gland would be located. However, for the child phantom, thyroid dose calculations were based on an average of two dosimeters in level 9 and one dosimeter in level 8. The rationale for this difference in dose measurement was based on the proximity of the thyroid gland to the lower border of the mandible, which is closer in children than in adults (Figure 12). This proximity means that direct exposure of the thyroid is more likely in children than in adults when the base of the FOV is situated just below the chin. In addition, the intensity of scatter radiation from jaw structures to the thyroid will also increase with the reduced distance of these structures in a child. Figures 13 and 14 are representative multi-planar renderings of the volumes taken of the child and adult phantoms during full FOV scans. With the thyroid positioned more superior in the child relative to the inferior border of the mandible, these images illustrate why it receives more radiation than that of the adult.

Since the thyroid has a tissue weight of 0.04, this organ provides a significant contribution to the calculation of effective dose for head and neck exposures. Clinically, direct thyroid exposure can be reduced by rotating the chin upward and positioning the lower border of the mandible parallel to the rotational plane of the beam (parallel to the floor). Unfortunately, this strategy was not possible due to the rigid phantoms used in this study. It is important to consider that for those concerned with cephalometric analyses, this technique would not place the patient's head in natural head position. Also, this strategy employs the use of a chin cup, which may cause difficulties for analyzing the soft tissue profile, chin, neck, and throat forms.

The use of CBCT units in orthodontics has been a controversial topic in recent history. In November 2010, a New York Times article expressed concern over the trend to use high-dose, high-resolution three-dimensional scans on young orthodontic patients.[66] Relevant to this issue, the results of our study demonstrate that effective doses were one-third greater in the child phantom than in the adult phantom. Compounding this greater dose of radiation is the fact that due to the increased radiosensitivity of tissues in children, the risk is an additional two to five times higher for a pediatric patient.[6] The relative risk of developing fatal cancer based on 2007 ICRP calculations, as a result of the effective doses seen in our study with the HD scans, equals 9 in a million for the adult and 27 in a million for the child.[8] The corresponding risk associated with developing thyroid cancer, based on the calculated equivalent doses in our study, equals 2 in a thousand for the adult and 11 in a thousand for the child. This is important information to consider when determining what type of diagnostic imaging might be best for a given patient.

The default exposure settings for the Galileos Comfort Plus unit are child exposure, HD on, full FOV. This is an important setting because inexperienced operators may utilize default settings without consideration of diagnostic task or patient size. For the child phantom, this

resulted in an effective dose of 122 μSv. When the HD off setting was selected for this same situation, the effective dose dropped to 39 μSv. Upon review of proper patient settings and FOV, our data demonstrate that optimization of exposure parameters can greatly reduce patient dose. In fact, the standard protocol (HD off) provided a substantial 67.2% reduction in dose compared to the high-definition scans in the child phantom, and a 66.9% reduction in dose in the adult phantom. Thus, when HD off protocols can be used, they will provide a clinically meaningful reduction in dose. The largest HD off dose in this study was 72 μSv for the full FOV, small adult setting (98 kVp, 10 mAs) on the child phantom. To put it into perspective, this dose is just over 8 days of per capita background radiation in the United States. It is also 28 times less than a typical medical CT head scan.[4]

As for the FOV options for the child phantom, the mandibular FOV provided a 20.3% reduction in dose compared to the full FOV, and the maxillary FOV provided a 41.4% reduction in dose compared to the full FOV. Similarly for the adult phantom, the average effective dose for the mandibular FOV was 15.0% less than the full FOV, and the maxillary FOV was 23.5% less than the full FOV. Therefore, if a full FOV scan is not necessary, a substantial decrease in radiation dose can be appreciated by the patient.

It is important to remember that in trying to lower the dose of ionizing radiation administered to patients, significant reductions are meaningless if image quality deteriorates to the point of not being diagnostic. As optimization and dose reduction become more of an emphasis for CBCT manufacturers, the effects on image quality will require attention. Evidence-based research establishing the usability of low-dose and low-quality scans for diagnostic purposes in orthodontics is limited. Having said that, a potential application could be a mid-treatment scan to evaluate root angulations, instead of the typical progress panoramic

radiograph. More studies are needed to support that other important information in two-dimensional imaging or higher-dose scans, e.g. periodontal conditions, changes in root length, and changes in morphology that could indicate root resorption, are not lost in these low-dose scans.

In August of 2013, the American Academy of Oral and Maxillofacial Radiology (AAOMR) released a position statement on their clinical recommendations regarding the use of CBCT in orthodontic treatment.[24] At the beginning of the statement, they listed diagnostic uses of CBCT in orthodontics, which include dental structural anomalies[25-30], anomalies in dental position[31-34], compromised dento-alveolar boundaries[35-37], asymmetry[38-40], anteroposterior discrepancies[41-43], vertical discrepancies[44, 45], transverse discrepancies[44, 46], TMJ signs and/or symptoms[47-49], dentofacial deformities and craniofacial anomalies[50-52], conditions that affect airway morphology[53-55], specific surgical procedures, orthodontic mini-implants used as temporary anchorage devices[56-58], and maxillary expanders.[59, 60] Then, they suggested four guidelines regarding the use of CBCT in orthodontic treatment. First, image appropriately according to the clinical situation. In other words, the decision to perform a CBCT examination should be based on the patient's history, clinical examination, available radiographic imaging, and the presence of a clinical condition for which the benefits to the diagnosis and treatment plan outweigh the risks of exposure to radiation, especially in the case of a child or young adult. They recommend avoiding the use of CBCT to obtain data that can be provided by alternative non-ionizing modalities, e.g., to produce virtual orthodontic study models. They also point out that few authors have presented higher levels of evidence and measured the impact of CBCT on orthodontic diagnosis and treatment planning decisions. One recent article looked at this topic and found that treatment plans were only affected in cases of unerupted teeth, severe root

resorption, and severe skeletal discrepancies. No benefit was found in cases where CBCT scans were used to examine abnormalities of the temporomandibular joint, airway space, or dental crowding.[61] Another study conducted dosimetry of the SureSmile (OraMetrix, Richardson, TX) scan protocol using an i-CAT Next Generation CBCT unit.[19] They found that a SureSmile scan of both arches in an adult imparts an effective dose of 148 μSv. This would correspond to an effective dose of between 148 and 198 μSv for the average pediatric orthodontic patient, according to Ludlow and Walker.[22] No research has been conducted to validate enhanced treatment outcomes associated with the SureSmile protocol, in defense of its increased radiation exposure. This leads to the second guideline from the AAOMR.

The second guideline is to assess the radiation dose risk. Orthodontists must be knowledgeable of the radiation risk of performing CBCT scans and be able to communicate this risk to their patients. Because CBCT exposes patients to ionizing radiation that may pose elevated risks to some patients (pregnant or younger patients), orthodontists must explain and disclose to patients the radiation exposure risks, benefits, and alternatives. Third, they recommend minimizing the patient radiation exposure. Specifically, one should perform CBCT imaging with acquisition parameters adjusted to the nominal settings consistent with providing appropriate images of task-specific diagnostic quality for the desired diagnostic information. Suggestions include using a pulsed exposure mode, optimizing exposure settings (mA, kVp), reducing the number of basis projection images, and employing dose reduction protocols (e.g., reduced resolution) when possible. In our study, we have illustrated how decreasing the mAs and reducing the number of basis images can greatly reduce the effective dose. Lastly, the AAOMR recommends maintaining professional competency in performing and interpreting CBCT studies. Orthodontists must be able to exercise judgment by applying professional

standards to all aspects of CBCT, while improving their skills through lifelong learning in regards to the performance and interpretation of CBCT examinations.

The AAOMR commented that CBCT acquisition technology continues to develop and a number of innovations are proposed to improve image quality, increase utility, and reduce radiation output. With regards to image quality, they advise that such innovations should be assessed critically and verified by independent published research.[24] The QUART DVT phantom is the first commercially available phantom to comply with standards for image quality testing of CBCT units. These standards were developed in Germany, which is where the phantom was manufactured. We evaluated the effect of the standard (HD off) and high-definition settings on the objective components of image quality contrast-to-noise ratio and modulation transfer function using the QUART DVT phantom. Our data demonstrated that as the milliamperes and basis images increased, the contrast-to-noise ratios increased as well. The average contrast-to-noise ratio was 4.0 for the high-definition scans, versus only 2.1 for the standard scans. Differences in contrast-to-noise ratio have been shown to generally correlate with observer impressions of an image.[67] As the contrast-to-noise ratio increases, the general impression of how an image appears improves. As expected, the modulation transfer function was not affected by the milliamperes or the basis images. The reduction of milliamperes and basis images from the high-definition to the standard settings reduced the effective dose to the phantoms by 67%, but only reduced the contrast-to-noise ratio by 50%. Thus, the reduction of milliamperes and basis images was an effective way to reduce patient dose in exchange for a modest reduction in the image quality, as measured by the contrast-to-noise ratio. In contrast, the objective measure of resolution, the modulation transfer function, was not as sensitive to the effects of milliamperes and basis images. Although contrast-to-noise ratio and modulation

transfer function can be correlated to subjective image quality, additional research to evaluate their influences on diagnostic efficacy is needed.[23]

CONCLUSIONS

1. Use of fewer basis images and smaller FOVs in the Galileos Comfort Plus unit result in significant patient dose reductions over alternative high-definition and larger FOVs settings.
2. Effective dose for a given FOV may be increased for pediatric patients due to an increase in thyroid exposure to ionizing radiation.
3. Contrast-to-noise ratio data in conjunction with modulation transfer function indications of resolution limits might be helpful guides in determining the usefulness of different scanning parameters for specific diagnostic tasks.

TABLES

Table 1. Scan parameters for Galileos Comfort Plus programs and exposure settings.

FOV	*HD*	*Program setting*	*kVp*	*mA*	*Phantom*
Full	On	Child	98	15	C
Full	On	Teen	98	20	A, C
Full	On	Small Adult	98	25	A, C
Full	On	Large Adult	98	30	A
Full	Off	Child	98	6	C
Full	Off	Teen	98	8	A, C
Full	Off	Small Adult	98	10	A, C
Full	Off	Large Adult	98	12	A
Maxilla	On	Child	98	15	C
Maxilla	On	Teen	98	20	A, C
Maxilla	On	Small Adult	98	25	A, C
Maxilla	On	Large Adult	98	30	A
Maxilla	Off	Child	98	6	C
Maxilla	Off	Teen	98	8	A, C
Maxilla	Off	Small Adult	98	10	A, C
Maxilla	Off	Large Adult	98	12	A
Mandible	On	Child	98	15	C
Mandible	On	Teen	98	20	A, C
Mandible	On	Small Adult	98	25	A, C
Mandible	On	Large Adult	98	30	A
Mandible	Off	Child	98	6	C
Mandible	Off	Teen	98	8	A, C
Mandible	Off	Small Adult	98	10	A, C
Mandible	Off	Large Adult	98	12	A

FOV, Field of view; *HD*, High-definition; *Phantom*: A, Adult; C, Child.

Table 2. Estimated percentage of tissue irradiated.

	Fraction Irradiated Adult (%)	*OSL ID (see Figure 1)*	*Fraction Irradiated Child (%)*	*OSL ID (see Figure 2)*
Bone marrow	12.2		15.4	
Mandible	0.8	14, 15	1.1	15, 16
Calvaria	7.7	1, 3, 5	11.6	1, 2, 3
Cervical spine	3.8	20	2.7	20
Thyroid	100	22, 23	100	21, 22, 23
Esophagus	10	24	10	24
Skin	5	7, 8, 16	5	8, 9, 14
Bone surface	16.5		16.5	
Mandible	1.3	14, 15	1.3	15, 16
Calvaria	11.8	1, 3, 5	11.8	1, 2, 3
Cervical spine	3.4	20	3.4	20
Salivary glands	100		100	
Parotid	100	12, 13	100	12, 13
Submandibular	100	17, 18	100	17, 18
Sublingual	100	19	100	19
Brain	100	2, 4, 6	100	4, 5, 6
Remainder				
Lymphatic nodes	5	11-13, 17-19, 21-24	5	12-13, 17-19, 21-24
Muscle	5	11-13, 17-19, 21-24	5	12-13, 17-19, 21-24
Extrathoracic region	100	9-13, 17-19, 21-24	100	10-13, 17-19, 21, 24
Oral mucosa	100	11-13, 17-19	100	12-13, 17-19

Table 3. Effective doses (μSv) for the child and adult phantoms by exposure protocol and field of view.

Child Phantom						
HD	OFF			ON		
mAs	6	8	10	15	20	25
Full	39	52	72	122	160	202
Man	29	44	55	99	136	159
Max	21	32	42	72	98	115
Adult Phantom						
HD	OFF			ON		
mAs	8	10	12	20	25	30
Full	36	47	61	112	140	168
Man	31	40	48	97	122	143
Max	28	36	43	86	111	133

OFF = 200 basis images; ON = 500 basis images.

Table 4. QUART phantom image measurements.

Scan setting	*Child*	*Teen*	*Sm Adult*	*Lg Adult*	*Child HD*	*Teen HD*	*Sm Adult HD*	*Lg Adult HD*
Basis images	200	200	200	200	500	500	500	500
kVp	98	98	98	98	98	98	98	98
mAs	6	8	10	12	15	20	25	30
Averages of 3 measurements								
PMMA Voxel	798.3	788.7	784.0	784.6	777.8	776.5	779.4	776.1
PMMA Noise	157.7	140.7	127.0	117.2	93.6	84.1	76.2	72.7
Homogeneity	9.3	15.3	20.7	21.0	20.0	22.0	20.0	26.0
Contrast	232.2	256.7	300.3	289.7	284.6	281.6	282.8	294.0
CNR	1.6	1.9	2.5	2.5	3.5	3.9	3.9	4.6
MTF 10%	1.4	1.5	1.5	1.5	1.5	1.5	1.5	1.5
MTF 50%	0.7	0.8	0.7	0.8	0.8	0.8	0.8	0.8
Nyquist Frequency	1.7	1.6	1.6	1.6	1.6	1.6	1.6	1.7
Standard deviations								
PMMA Voxel	27.5	3.2	4.8	3.2	3.0	4.3	8.6	3.7
PMMA Noise	12.8	1.3	2.0	0.9	1.1	1.3	2.8	1.1
Homogeneity	7.0	3.8	5.1	6.2	4.4	5.2	10.5	8.7
Contrast	139.5	65.1	74.2	67.0	54.7	42.6	80.2	88.0
CNR	0.8	0.5	0.6	0.2	0.8	0.4	1.2	1.0
MTF 10%	0.3	0.2	0.1	0.2	0.0	0.1	0.1	0.1
MTF 50%	0.1	0.1	0.0	0.1	0.1	0.1	0.1	0.1
Nyquist Frequency	0.0	0.0	0.0	0.0	0.0	0.0	0.0	0.0

PMMA, Polymethylmethacrylate; *CNR,* contrast-to-noise ratio; *MTF,* modulation transfer function.

FIGURES

Figure 1. Adult phantom dosimeter locations.

OSL ID No.	Adult phantom location (level of OSLD location)
1	Calvarium anterior (2)
2	Mid brain (2)
3	Calvarium left (3)
4	Mid brain (3)
5	Calvarium posterior (4)
6	Pituitary (4)
7	Right lens of eye (4-5)
8	Left lens of eye (4-5)
9	Right ethmoid (5)
10	Left maxillary sinus (6)
11	Oropharyngeal airway (7)
12	Right parotid (7)
13	Left parotid (7)
14	Right ramus (7)
15	Left ramus (7)
16	Left back of neck (8)
17	Right submandibular gland (8)
18	Left submandibular gland (8)
19	Center sublingual gland (8)
20	Center C spine (8)
21	Lateral neck - left (9)
22	Thyroid – left (10)
23	Thyroid - right (10)
24	Esophagus (10)

Phantom Levels

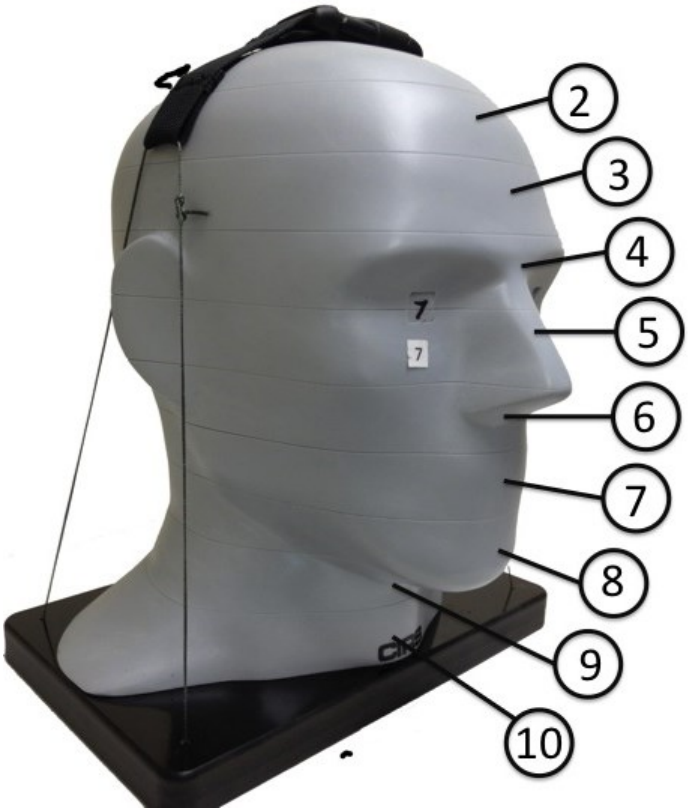

Figure 2. Child phantom dosimeter locations.

OSL ID No.	Child phantom location (level of OSLD location)
1	Calvarium anterior (2)
2	Calvarium left (2)
3	Calvarium posterior (2)
4	Mid brain (2)
5	Mid brain (3)
6	Pituitary (4)
7	Right orbit (4)
8	Right lens of eye (4-5)
9	Left lens of eye (4-5)
10	Right maxillary sinus (5)
11	Left nasal airway (5)
12	Right parotid (6)
13	Left parotid (6)
14	Left back of neck (6)
15	Right ramus (7)
16	Left ramus (7)
17	Right submandibular gland (7)
18	Left submandibular gland (7)
19	Center sublingual gland (7)
20	Center C spine (8)
21	Thyroid superior–left (8)
22	Thyroid – left (9)
23	Thyroid – right (9)
24	Esophagus (9)

Phantom Levels

Figure 3. QUART DVT_AP phantom.

Figure 4. Effective doses for the child and adult phantoms at the same high-definition settings.

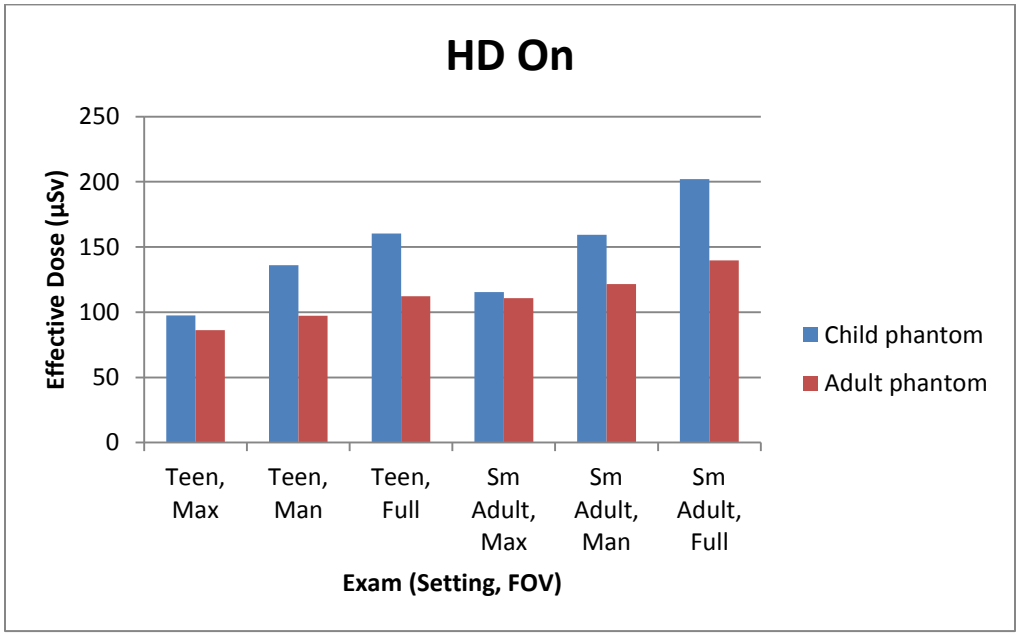

Figure 5. Effective doses for the child and adult phantoms at the same standard settings.

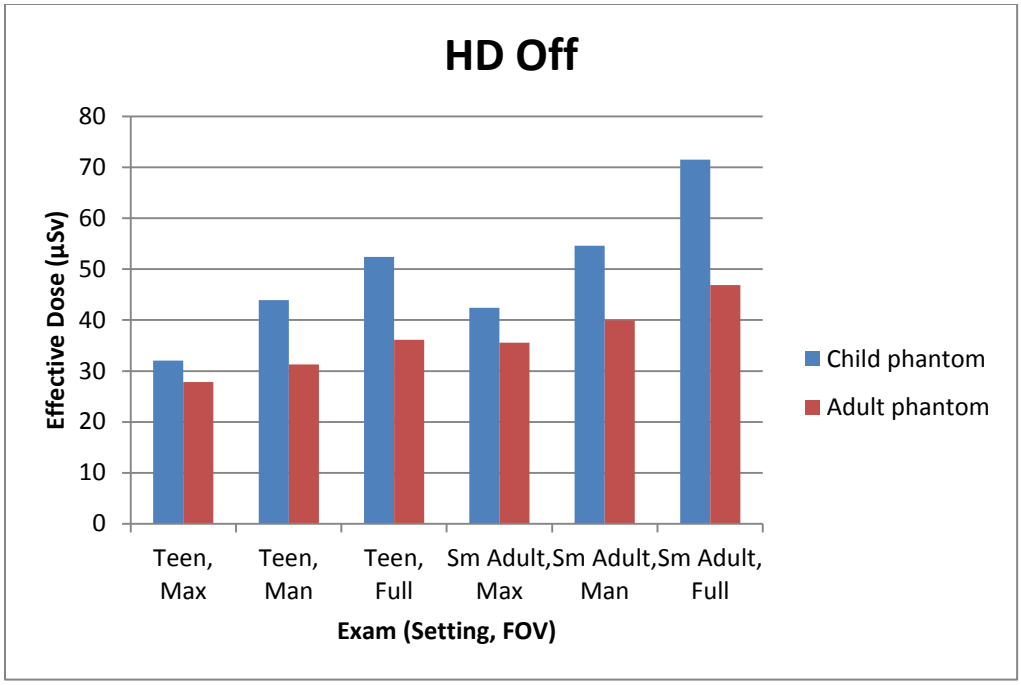

Figure 6. Effective doses for the child phantom at the high-definition settings.

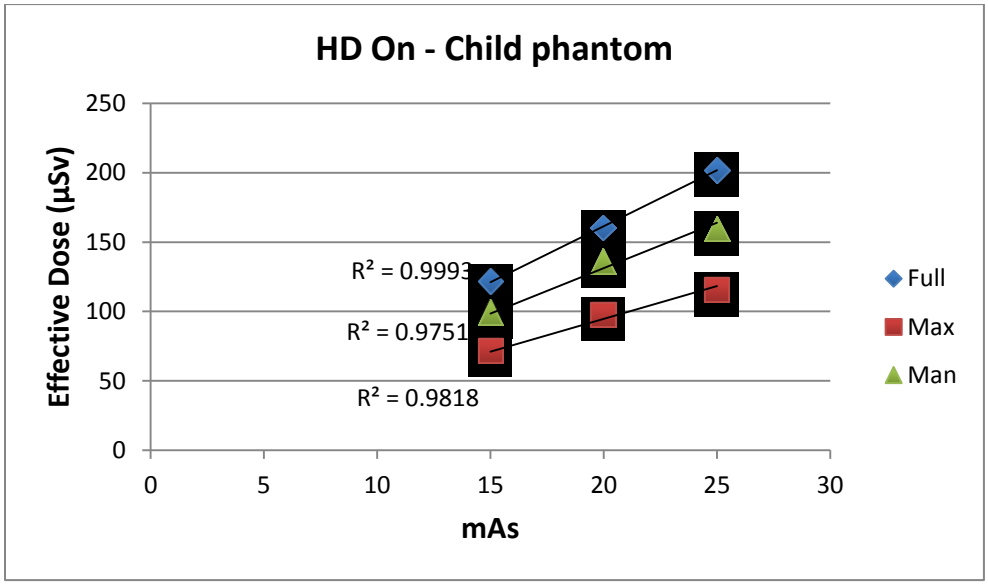

Figure 7. Effective doses for the child phantom at the standard settings.

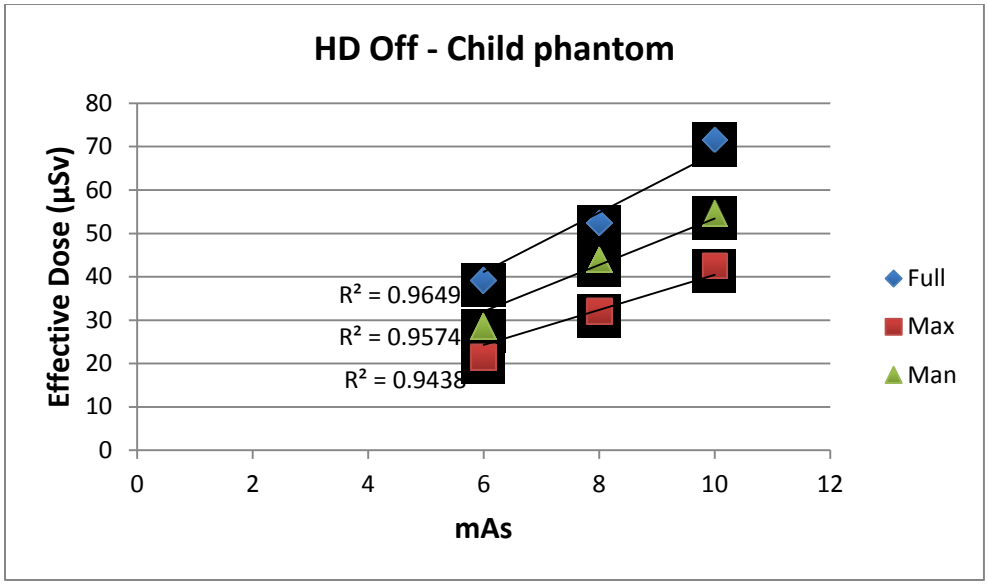

Figure 8. Effective doses for the adult phantom at the high-definition settings.

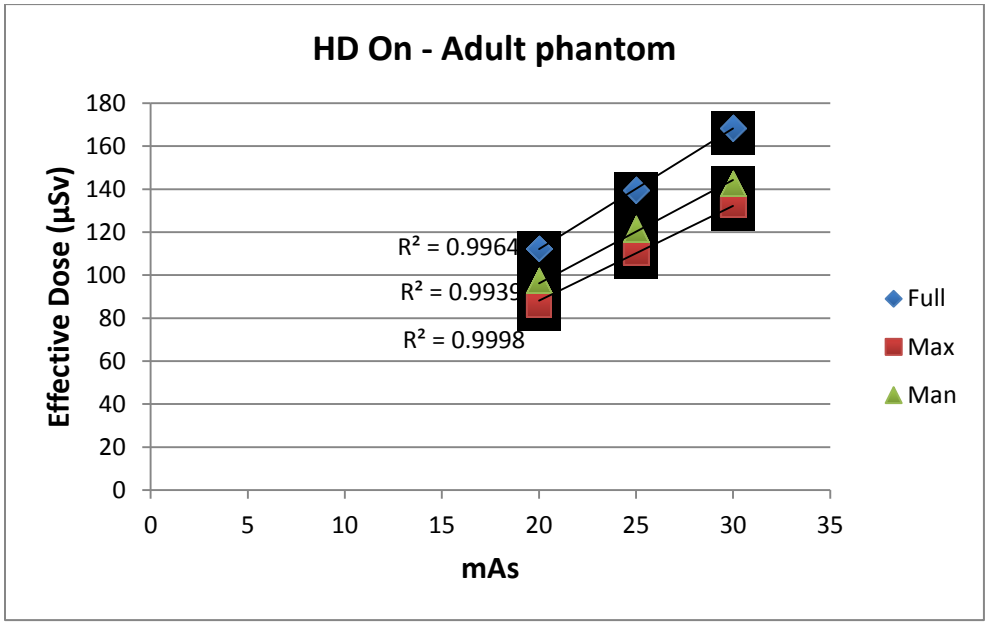

Figure 9. Effective doses for the adult phantom at the standard settings.

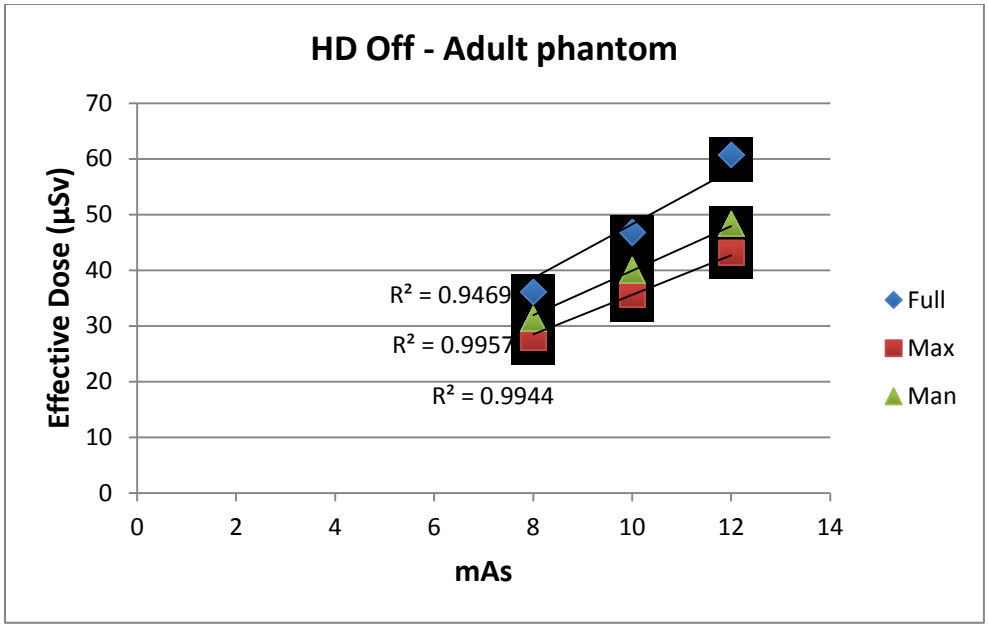

Figure 10. Equivalent dose measurements (µGy) for the child phantom.

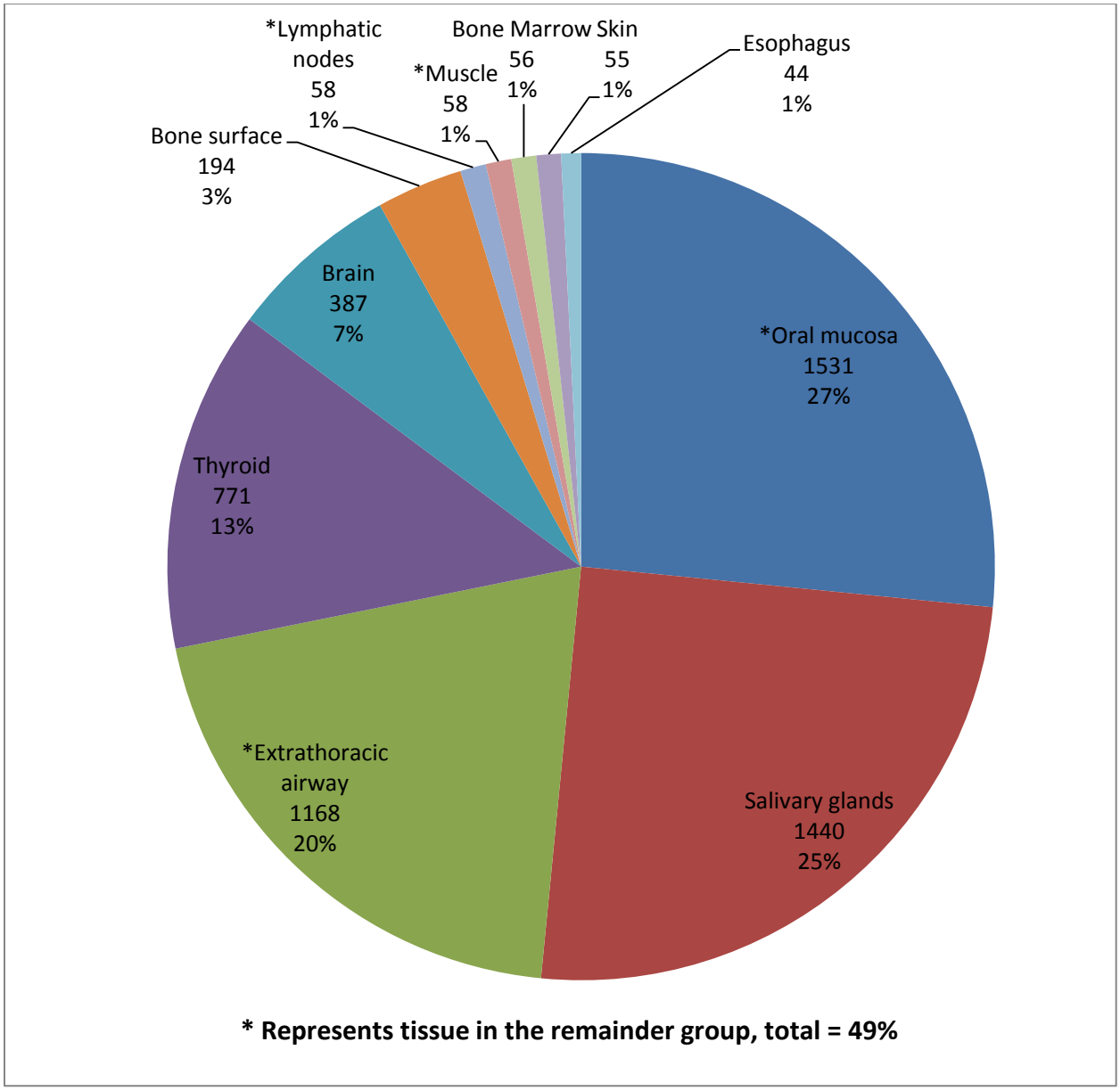

Figure 11. Equivalent dose measurements (µGy) for the adult phantom.

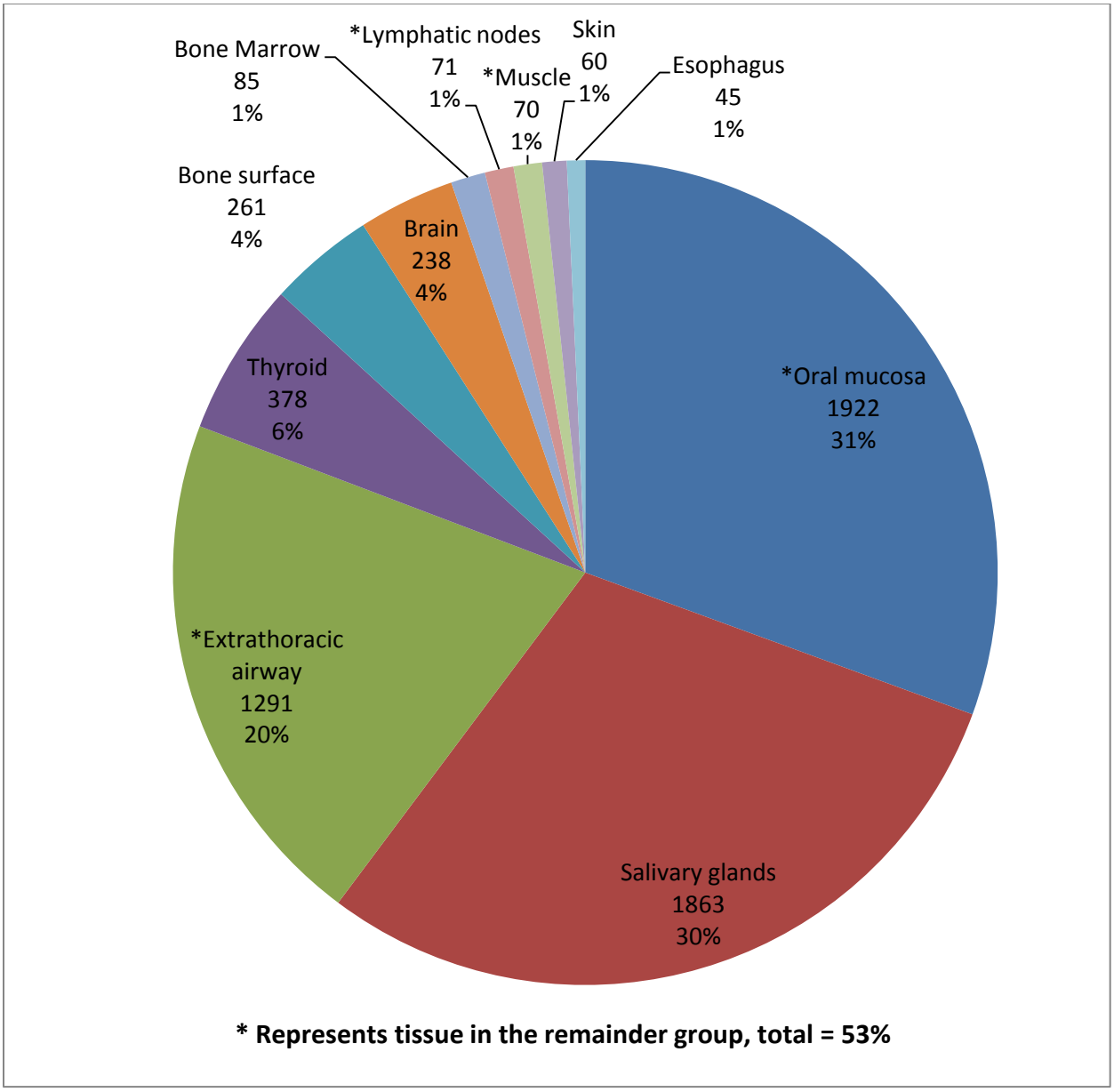

Figure 12. Comparison of thyroid level in child and adult.

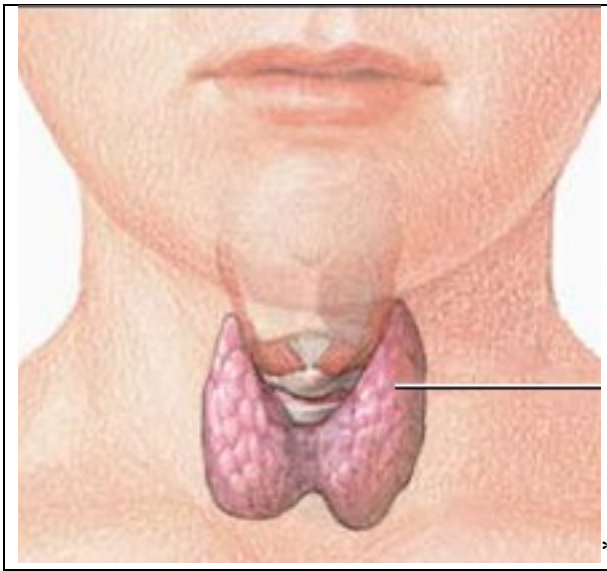

Thyroid position in child

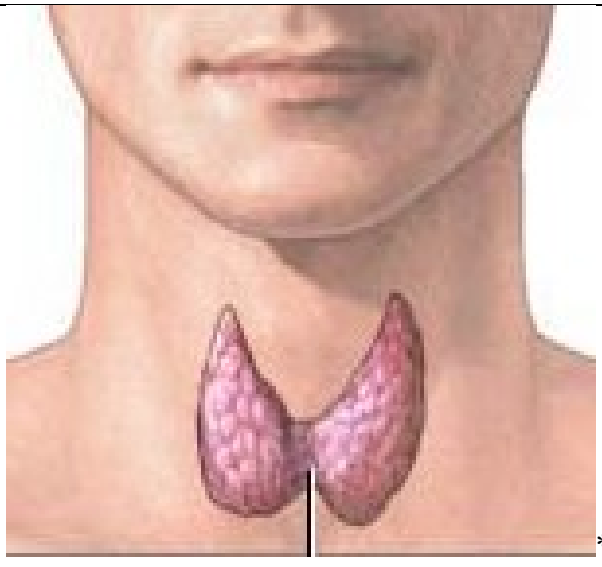

Thyroid position in adult

* A.D.A.M. medical images http://www.adamimages.com

Figure 13. Positioning of the child phantom for the full field of view scan.

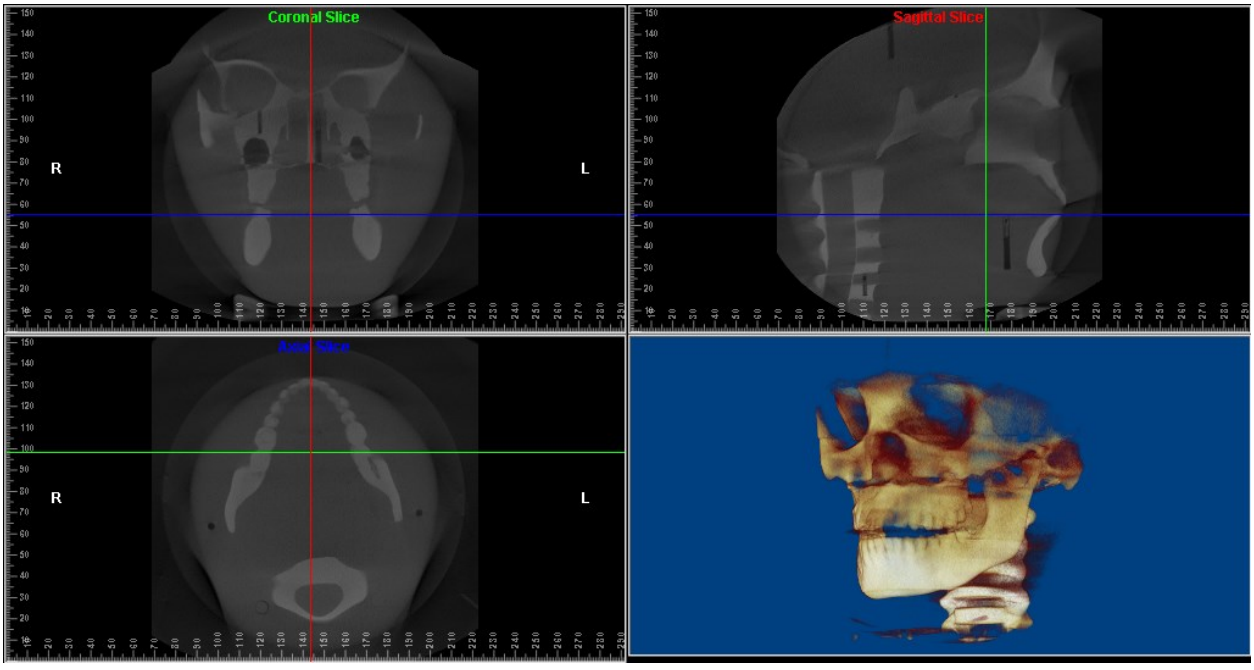

Figure 14. Positioning of the adult phantom for the full field of view scan.

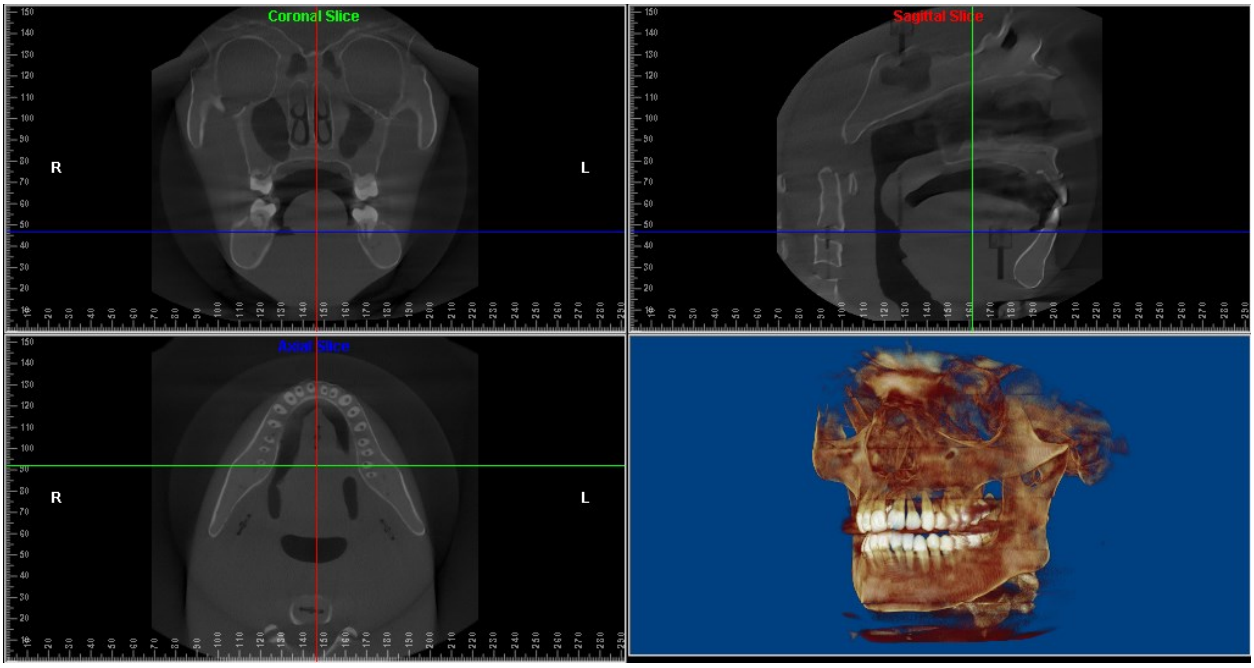

REFERENCES

1. Ionizing radiation exposure of the population of the United States: Recommendations of the national council on radiation protection and measurements. NCRP Publications; 2009. Report nr 160.

2. Brenner DJ, Hall EJ. Computed tomography--an increasing source of radiation exposure. N Engl J Med 2007 Nov 29;357(22):2277-84.

3. Goaz PW WS, editor. Oral radiology, principles and interpretation. 3rd edition ed. St. Louis: Mosby; 1994.

4. Smith-Bindman R, Lipson J, Marcus R, Kim KP, Mahesh M, Gould R, Berrington de Gonzalez A, Miglioretti DL. Radiation dose associated with common computed tomography examinations and the associated lifetime attributable risk of cancer. Arch Intern Med 2009 Dec 14;169(22):2078-86.

5. Ludlow JB, Ivanovic M. Comparative dosimetry of dental CBCT devices and 64-slice CT for oral and maxillofacial radiology. Oral Surg Oral Med Oral Pathol Oral Radiol Endod 2008 Jul;106(1):106-14.

6. Brenner D, Elliston C, Hall E, Berdon W. Estimated risks of radiation-induced fatal cancer from pediatric CT. AJR Am J Roentgenol 2001 Feb;176(2):289-96.

7. 1990 recommendations of the international commission on radiological protection. ICRP publication 60; Ann ICRP 1991.

8. The 2007 recommendations of the international commission on radiological protection. ICRP publication 103. Ann ICRP 2007;37(2-4):1-332.

9. Ludlow JB, Davies-Ludlow LE, White SC. Patient risk related to common dental radiographic examinations: The impact of 2007 international commission on radiological protection recommendations regarding dose calculation. J Am Dent Assoc 2008 Sep;139(9):1237-43.

10. Scarfe WC, Farman AG, Sukovic P. Clinical applications of cone-beam computed tomography in dental practice. J can Dent Assoc 2006 Feb;72(1):75-80.

11. Thomas SL. Application of cone-beam CT in the office setting. Dent Clin North Am 2008 Oct;52(4):753,9, vi.

12. Mussig E, Wortche R, Lux CJ. Indications for digital volume tomography in orthodontics. J Orofac Orthop 2005 May;66(3):241-9.

13. Hechler SL. Cone-beam CT: Applications in orthodontics. Dent Clin North Am 2008 Oct;52(4):809,23, vii.

14. White SC PE. Patient image selection criteria for cone beam computed tomography imaging. Semin Orthod 2009(15):19-28.

15. Merrett SJ, Drage NA, Durning P. Cone beam computed tomography: A useful tool in orthodontic diagnosis and treatment planning. J Orthod 2009 Sep;36(3):202-10.

16. Mah JK, Huang JC, Choo H. Practical applications of cone-beam computed tomography in orthodontics. J Am Dent Assoc 2010 Oct;141 Suppl 3:7S-13S.

17. Kapila S, Conley RS, Harrell WE,Jr. The current status of cone beam computed tomography imaging in orthodontics. Dentomaxillofac Radiol 2011 Jan;40(1):24-34.

18. Nervina JM. Cone beam computed tomography use in orthodontics. Aust Dent J 2012 Mar;57 Suppl 1:95-102.

19. Grunheid T, Kolbeck Schieck JR, Pliska BT, Ahmad M, Larson BE. Dosimetry of a cone-beam computed tomography machine compared with a digital x-ray machine in orthodontic imaging. Am J Orthod Dentofacial Orthop 2012 Apr;141(4):436-43.

20. Pauwels R, Beinsberger J, Collaert B, Theodorakou C, Rogers J, Walker A, Cockmartin L, Bosmans H, Jacobs R, Bogaerts R, et al. Effective dose range for dental cone beam computed tomography scanners. Eur J Radiol 2012 Feb;81(2):267-71.

21. Ludlow JB. Comment on "effective dose range for dental cone beam computed tomography scanners". Eur J Radiol 2012 Dec;81(12):4219,20; author reply 4221-4.

22. Ludlow JB, Walker C. Assessment of phantom dosimetry and image quality of i-CAT FLX cone-beam computed tomography. Am J Orthod Dentofacial Orthop 2013 Dec;144(6):802-17.

23. Watanabe H, Honda E, Tetsumura A, Kurabayashi T. A comparative study for spatial resolution and subjective image characteristics of a multi-slice CT and a cone-beam CT for dental use. Eur J Radiol 2011 Mar;77(3):397-402.

24. American Academy of Oral and Maxillofacial Radiology. Clinical recommendations regarding use of cone beam computed tomography in orthodontics. [corrected]. position statement by the american academy of oral and maxillofacial radiology. Oral Surg Oral Med Oral Pathol Oral Radiol 2013 Aug;116(2):238-57.

25. Peck JL, Sameshima GT, Miller A, Worth P, Hatcher DC. Mesiodistal root angulation using panoramic and cone beam CT. Angle Orthod 2007 Mar;77(2):206-13.

26. Liu DG, Zhang WL, Zhang ZY, Wu YT, Ma XC. Three-dimensional evaluations of supernumerary teeth using cone-beam computed tomography for 487 cases. Oral Surg Oral Med Oral Pathol Oral Radiol Endod 2007 Mar;103(3):403-11.

27. Sherrard JF, Rossouw PE, Benson BW, Carrillo R, Buschang PH. Accuracy and reliability of tooth and root lengths measured on cone-beam computed tomographs. Am J Orthod Dentofacial Orthop 2010 Apr;137(4 Suppl):S100-8.

28. Katheria BC, Kau CH, Tate R, Chen JW, English J, Bouquot J. Effectiveness of impacted and supernumerary tooth diagnosis from traditional radiography versus cone beam computed tomography. Pediatr Dent 2010 Jul-Aug;32(4):304-9.

29. Van Elslande D, Heo G, Flores-Mir C, Carey J, Major PW. Accuracy of mesiodistal root angulation projected by cone-beam computed tomographic panoramic-like images. Am J Orthod Dentofacial Orthop 2010 Apr;137(4 Suppl):S94-9.

30. Makedonas D, Lund H, Hansen K. Root resorption diagnosed with cone beam computed tomography after 6 months and at the end of orthodontic treatment with fixed appliances. Angle Orthod 2013 May;83(3):389-93.

31. Chaushu S, Chaushu G, Becker A. The role of digital volume tomography in the imaging of impacted teeth. World J Orthod 2004 Summer;5(2):120-32.

32. Walker L, Enciso R, Mah J. Three-dimensional localization of maxillary canines with cone-beam computed tomography. Am J Orthod Dentofacial Orthop 2005 Oct;128(4):418-23.

33. Guerrero ME, Shahbazian M, Elsiena Bekkering G, Nackaerts O, Jacobs R, Horner K. The diagnostic efficacy of cone beam CT for impacted teeth and associated features: A systematic review. J Oral Rehabil 2011 Mar;38(3):208-16.

34. Nguyen E, Boychuk D, Orellana M. Accuracy of cone-beam computed tomography in predicting the diameter of unerupted teeth. Am J Orthod Dentofacial Orthop 2011 Aug;140(2):e59-66.

35. Rungcharassaeng K, Caruso JM, Kan JY, Kim J, Taylor G. Factors affecting buccal bone changes of maxillary posterior teeth after rapid maxillary expansion. Am J Orthod Dentofacial Orthop 2007 Oct;132(4):428.e1,428.e8.

36. Loubele M, Van Assche N, Carpentier K, Maes F, Jacobs R, van Steenberghe D, Suetens P. Comparative localized linear accuracy of small-field cone-beam CT and multislice CT for alveolar bone measurements. Oral Surg Oral Med Oral Pathol Oral Radiol Endod 2008 Apr;105(4):512-8.

37. Yagci A, Veli I, Uysal T, Ucar FI, Ozer T, Enhos S. Dehiscence and fenestration in skeletal class I, II, and III malocclusions assessed with cone-beam computed tomography. Angle Orthod 2012 Jan;82(1):67-74.

38. Sievers MM, Larson BE, Gaillard PR, Wey A. Asymmetry assessment using cone beam CT. A class I and class II patient comparison. Angle Orthod 2012 May;82(3):410-7.

39. AlHadidi A, Cevidanes LH, Mol A, Ludlow J, Styner M. Comparison of two methods for quantitative assessment of mandibular asymmetry using cone beam computed tomography image volumes. Dentomaxillofac Radiol 2011 Sep;40(6):351-7.

40. Cevidanes LH, Alhadidi A, Paniagua B, Styner M, Ludlow J, Mol A, Turvey T, Proffit WR, Rossouw PE. Three-dimensional quantification of mandibular asymmetry through cone-beam computerized tomography. Oral Surg Oral Med Oral Pathol Oral Radiol Endod 2011 Jun;111(6):757-70.

41. Tucker S, Cevidanes LH, Styner M, Kim H, Reyes M, Proffit W, Turvey T. Comparison of actual surgical outcomes and 3-dimensional surgical simulations. J Oral Maxillofac Surg 2010 Oct;68(10):2412-21.

42. Heymann GC, Cevidanes L, Cornelis M, De Clerck HJ, Tulloch JF. Three-dimensional analysis of maxillary protraction with intermaxillary elastics to miniplates. Am J Orthod Dentofacial Orthop 2010 Feb;137(2):274-84.

43. Kim YI, Park SB, Son WS, Hwang DS. Midfacial soft-tissue changes after advancement of maxilla with le fort I osteotomy and mandibular setback surgery: Comparison of conventional and high le fort I osteotomies by superimposition of cone-beam computed tomography volumes. J Oral Maxillofac Surg 2011 Jun;69(6):e225-33.

44. Lagravere MO, Carey J, Heo G, Toogood RW, Major PW. Transverse, vertical, and anteroposterior changes from bone-anchored maxillary expansion vs traditional rapid maxillary expansion: A randomized clinical trial. Am J Orthod Dentofacial Orthop 2010 Mar;137(3):304.e1,12; discussion 304-5.

45. Kim YI, Choi YK, Park SB, Son WS, Kim SS. Three-dimensional analysis of dental decompensation for skeletal class III malocclusion on the basis of vertical skeletal patterns obtained using cone-beam computed tomography. Korean J Orthod 2012 Oct;42(5):227-34.

46. Miner RM, Al Qabandi S, Rigali PH, Will LA. Cone-beam computed tomography transverse analysis. part I: Normative data. Am J Orthod Dentofacial Orthop 2012 Sep;142(3):300-7.

47. Hilgers ML, Scarfe WC, Scheetz JP, Farman AG. Accuracy of linear temporomandibular joint measurements with cone beam computed tomography and digital cephalometric radiography. Am J Orthod Dentofacial Orthop 2005 Dec;128(6):803-11.

48. Cevidanes LH, Hajati AK, Paniagua B, Lim PF, Walker DG, Palconet G, Nackley AG, Styner M, Ludlow JB, Zhu H, et al. Quantification of condylar resorption in temporomandibular joint osteoarthritis. Oral Surg Oral Med Oral Pathol Oral Radiol Endod 2010 Jul;110(1):110-7.

49. Palconet G, Ludlow JB, Tyndall DA, Lim PF. Correlating cone beam CT results with temporomandibular joint pain of osteoarthritic origin. Dentomaxillofac Radiol 2012 Feb;41(2):126-30.

50. Swennen GR, Mollemans W, De Clercq C, Abeloos J, Lamoral P, Lippens F, Neyt N, Casselman J, Schutyser F. A cone-beam computed tomography triple scan procedure to obtain a three-dimensional augmented virtual skull model appropriate for orthognathic surgery planning. J Craniofac Surg 2009 Mar;20(2):297-307.

51. Carvalho Fde A, Cevidanes LH, da Motta AT, Almeida MA, Phillips C. Three-dimensional assessment of mandibular advancement 1 year after surgery. Am J Orthod Dentofacial Orthop 2010 Apr;137(4 Suppl):S53.e1,12; discussion S53-5.

52. da Motta AT, de Assis Ribeiro Carvalho F, Oliveira AE, Cevidanes LH, de Oliveira Almeida MA. Superimposition of 3D cone-beam CT models in orthognathic surgery. Dental Press J Orthod 2010 Mar 1;15(2):39-41.

53. Aboudara CA, Hatcher D, Nielsen IL, Miller A. A three-dimensional evaluation of the upper airway in adolescents. Orthod Craniofac Res 2003;6 Suppl 1:173-5.

54. Oh KM, Hong JS, Kim YJ, Cevidanes LS, Park YH. Three-dimensional analysis of pharyngeal airway form in children with anteroposterior facial patterns. Angle Orthod 2011 Nov;81(6):1075-82.

55. Alsufyani NA, Flores-Mir C, Major PW. Three-dimensional segmentation of the upper airway using cone beam CT: A systematic review. Dentomaxillofac Radiol 2012 May;41(4):276-84.

56. Baumgaertel S, Hans MG. Buccal cortical bone thickness for mini-implant placement. Am J Orthod Dentofacial Orthop 2009 Aug;136(2):230-5.

57. Kau CH, English JD, Muller-Delgardo MG, Hamid H, Ellis RK, Winklemann S. Retrospective cone-beam computed tomography evaluation of temporary anchorage devices. Am J Orthod Dentofacial Orthop 2010 Feb;137(2):166.e1,5; discussion 166-7.

58. Qiu L, Haruyama N, Suzuki S, Yamada D, Obayashi N, Kurabayashi T, Moriyama K. Accuracy of orthodontic miniscrew implantation guided by stereolithographic surgical stent based on cone-beam CT-derived 3D images. Angle Orthod 2012 Mar;82(2):284-93.

59. Garrett BJ, Caruso JM, Rungcharassaeng K, Farrage JR, Kim JS, Taylor GD. Skeletal effects to the maxilla after rapid maxillary expansion assessed with cone-beam computed tomography. Am J Orthod Dentofacial Orthop 2008 Jul;134(1):8-9.

60. Domann CE, Kau CH, English JD, Xia JJ, Souccar NM, Lee RP. Cone beam computed tomography analysis of dentoalveolar changes immediately after maxillary expansion. Orthodontics (Chic) 2011 Fall;12(3):202-9.

61. Hodges RJ, Atchison KA, White SC. Impact of cone-beam computed tomography on orthodontic diagnosis and treatment planning. Am J Orthod Dentofacial Orthop 2013 May;143(5):665-74.

62. Underhill TE, Chilvarquer I, Kimura K, Langlais RP, McDavid WD, Preece JW, Barnwell G. Radiobiologic risk estimation from dental radiology. part I. absorbed doses to critical organs. Oral Surg Oral Med Oral Pathol 1988 Jul;66(1):111-20.

63. Cristy M. Active bone marrow distribution as a function of age in humans. Phys Med Biol 1981 May;26(3):389-400.

64. ROBERTSON DF. Physical aspects of acute radiation exposure to superficial tissue. J Coll Radiol Australas 1963 Oct;7:214-6.

65. Ludlow JB, Davies-Ludlow LE, Brooks SL. Dosimetry of two extraoral direct digital imaging devices: NewTom cone beam CT and orthophos plus DS panoramic unit. Dentomaxillofac Radiol 2003 Jul;32(4):229-34.

66. Bogdanich W, Craven McGinty J. Radiation worries for children in dentists' chairs. The New York Times(NY ed) . 2010 Nov 23 2010;.

67. Lin Y, Wang X, Sehnert W, Foos D, Barski L, Samei E. Quantification of radiographic image qualtiy based on patient anatomical contrast-to-noise ratio: A preliminary study with chest images. Image Perception, Observer Performance, and Technology Assessment: Medical Imaging 2010; 2010. Report nr Proc. SPIE 7627.